Nuclear Engineering and Technology 53 (2021) 3643–3652

Contents lists available at ScienceDirect

Nuclear Engineering and Technology

journal homepage: www.elsevier.com/locate/net

Original Article

Sizing of a tube inlet orifice of a once-through steam generator to suppress the parallel channel instability

Juhyeon Yoon

Korea Atomic Energy Research Institute, 989-111 Daedeok-daero, Yuseong, Daejeon, 34057, Republic of Korea

ARTICLE INFO

Article history:
Received 30 March 2021
Received in revised form
1 June 2021
Accepted 2 June 2021
Available online 16 June 2021

Keywords:
Once-through steam generator (OTSG)
Parallel channel instability
Stability threshold
Orifice
Perturbation method

ABSTRACT

Sizing the tube inlet orifice of a Once-Through Steam Generator (OTSG) is important to protect the integrity of the tubes from thermal cycling and vibration wear. In this study, a new sizing criterion is proposed for the tube inlet orifice to suppress the parallel channel instability in an OTSG. A perturbation method is used to capture the essential parts of the thermal-hydraulic phenomena of the parallel channel instability. The perturbation model of the heat transfer regime boundaries is identified as a missing part in existing models for sizing the OTSG tube inlet orifice. Limitations and deficiency of the existing models are identified and the reasons for the limitations are explained. The newly proposed model can be utilized to size the tube inlet orifice to suppress the parallel channel instability without excessive engineering margin.

1. Introduction

A new stability threshold model is presented in terms of the necessary pressure drop at the tube inlet orifice of an OTSG to suppress the parallel channel instability. Usually, an OTSG has many steam generating tubes coupled by common headers at both inlet and outlet ends. This kind of multichannel structure is more susceptible to flow instability than in a single boiling channel [1,2]. The parallel channel instability is classified as a compound dynamic instability caused by interaction between the multichannel and density wave oscillation, and the term 'parallel channel' is frequently used to imply a constant pressure drop boundary condition [3–5].

Various operating parameters affect the two-phase flow instability in an OTSG, like the steam pressure, inlet mass velocity, inlet subcooling, heat flux, and inlet and outlet geometrical restrictions [3,6–8]. In the steam generator designer's point of view, all other operating parameters are predetermined by plant design requirements, except the inlet and outlet orifice sizes for the flow restrictions. It is well known that the tube inlet single-phase pressure drop stabilizes and the outlet flow restriction destabilizes the boiling flow. It is because the inlet single-phase pressure drop is in-phase with the inlet flow rate change and provides a damping effect on the increasing flow, but the outlet flow restriction increases the superheater region pressure drop which is out of phase with the inlet flow rate change [3,6,7]. Thus, a steam generator designer wants to install an orifice for a large pressure drop at each steam generating tube inlet for a stable operation of the steam generator. However, these orifices will increase the irreversible pressure drop of the steam generator secondary side. It will require a high specification of the feedwater pump and increase the total operating cost for the plant lifetime. Thus, installing the right size of the tube inlet orifice is essential.

Many researches have been performed to identify the stability boundary of boiling channels. Most of the studies focused on boiling channels in which the exit quality is less than one, which is corresponding to the Boiling Water Reactor (BWR) core [6,9–16,27]. The BWR core has many closed fuel assembly channels coupled to common headers at both inlet and outlet ends. In the flow instability point of view, the geometrical structure of the BWR core is very similar with that of the OTSG, except that the BWR core heats the coolant up to the exit quality less than one, while the OTSG produces superheated steam. Many stability threshold models are presented for the BWR core [6,9,13,14], but these models cannot be utilized for the OTSG inlet orifice sizing purpose for the reasons explained below.

The OTSG becomes hydrodynamically more unstable, when the steam pressure and the inlet mass velocity decrease [3,6–8]. Thus, the steam generator tube inlet orifice should be sized based on the

E-mail address: yoonj@kaeri.re.kr.

https://doi.org/10.1016/j.net.2021.06.003

normal operating condition which has the lowest steam pressure and inlet flow rate, for which the steam generator should be guaranteed for a stable operation. In this operating condition, most inside part of the steam generating tube is occupied by the superheater region, and the superheater region pressure drop is order of magnitude larger than the economizer and evaporator region pressure drops. For this operating condition, the tube inlet orifice pressure drop (in-phase damping force) and the superheater region pressure drop (feedback driving force) are the dominant players in the OTSG flow instability. This explains many stability threshold models developed for the BWR core stability map, which do not have the superheater region model, have limitations for the OTSG orifice design purpose.

Takitani et al. [10–12] performed in-depth researches on the density wave instability in a once-through boiling flow system including the superheater region. Their experimental facility has two parallel tubes with a bypass flow path to impose the constant pressure drop boundary condition. They obtained the stability boundary by comparing experimental data [10], simplified lumped parameter model [11] and calculated results from a computer code developed especially for a comprehensive distributed parameter model [12]. The stability map is presented in the plane of the mass flux covering the 500–900 kg/m^2/s range and the y-value representing the fraction of the total pressure loss attributable to the subcooled region. The code calculated results predicted the experimental results well, however, the lumped parameter model prediction showed appreciable deviation in prediction of the stability map compared with experimental results [12]. Advanced pressurized water reactors being developed nowadays have a wide range of operating power range for a load following operation to match the renewable energy variability, and the target minimum feedwater flow rate for the OTSG stability design is usually around the 100 kg/m^2/s or less, which is out of range in the presented stability map. Recently, Xu, et al. [17] developed a dynamic analysis computer code for time-domain numerical analysis of the parallel channel instability for a sodium-cooled fast reactor OTSG. They obtained a stability map in the $N_{pch} - N_{sub}$ plane and analysed the effects of system pressure, inlet subcooling, inlet mass flow rate and the sodium side inlet temperature and flow rate. Liang et al. [18] extended the frequency domain model to include the superheater region for the HTGR OTSG. They obtained the two-phase instability boundary for a helical OTSG for the range of 30–100% power levels, where the 30% rated power level is rather too high for the reactor operation for startup and load-following purposes.

Utilizing a dynamic analysis computer code for sizing the OTSG tube inlet orifice requires lots of analyses to find the boundary between the growth and decay of flow perturbations with varying the orifice size and system parameters. Furthermore, it requires lots of efforts to make the dynamic computer code converged for physically unstable problems. Because of many involved tuning to make the code converged, validation of the code and model against experimental data is essential. Alternatively, the threshold of the flow instability can be derived by using a perturbation method and two stability thresholds derived from the perturbation method are available.

Petrov [19–22] derived a stability threshold by considering the damping effect of the single-phase region pressure drop including the tube inlet orifice pressure drop and the feedback driving force of the two-phase and superheater region pressure drops. His threshold tells the sum of the tube inlet orifice and economizer region pressure drops must be equal to or greater than the sum of two-phase and superheater region pressure drops to suppress the flow instability for a constant pressure drop channels. The Petrov's criterion requires too much ambiguous margin in application for sizing the OTSG tube inlet orifice based on experience and experimental data [20–23]. Nariai et al. [24] performed extensive experiments to investigate flow instabilities in an OTSG and analysed the experimental data using the perturbation theory model. They presented a stability threshold expressed in the ratio of the orifice pressure drop to the sum of the evaporator and superheater region pressure drops. The ratio can be calculated with presented formulas and graphical data which are fitted by using their test data. When Nariai's threshold is applied for sizing the OTSG tube inlet orifice, the presented formula and graphical data do not cover the low power range for practical design purpose.

This paper presents a new stability threshold which is applicable for practical design purpose and does not require excessive engineering margin. The Petrov's and Nariai's stability thresholds are evaluated in detail in the discussion section.

2. Model development

For a mathematical modelling purpose, two parallel steam generating identical tubes are modelled as connected by inlet and outlet common headers as shown in Fig. 1. The inlet and outlet common headers are assumed to have constant pressures. For model simplification, a constant and uniform tube wall heat flux is assumed and it is a common practice for derivation of an analytical model for the analysis of density-wave oscillations [11,13,16,25,26,27]. Constant inlet subcooling is also assumed. Each tube has an orifice installed at the tube inlet to suppress the parallel channel instability. Each tube has a fixed total length which is subdivided into economizer, evaporator and superheater heat transfer regions. The boiling and superheat boundaries are defined by the points where the mixture mean enthalpy reaches that of saturated liquid and that of vapor, respectively. The (a1) and (a2) tubes in Fig. 1 represent an imaginary steady state condition for modelling purpose without any perturbations. For this steady state, the total feedwater and steam flowrate through the two tubes is assumed to be constant with a constant pressure drop boundary condition between the two common headers. The (b1) and (b2) tubes represent an instantaneous perturbed condition which has one tube with a positive inlet flow perturbation and another one with a negative inlet flow perturbation. Because of the time delay of the void wave and the constant pressure drop boundary condition between the common headers, the inlet feedwater flowrate perturbation and outlet steam flowrate perturbation are assumed to have 180° out-of-phase [3,4,11,13,24,26]. For a modelling purpose, part (β) of the evaporator region pressure drop perturbation is assumed to be in-phase with the inlet feedwater flowrate perturbation, and other part ($1 - \beta$) of the evaporator region pressure drop perturbation is assumed to be in-phase with the outlet steam flowrate perturbation [24]. The pressure at the imaginary boundary is assigned to be p_{IP} as shown in the (b1) tube in Fig. 1.

The essential physical phenomenon of the density wave oscillation is competing between the damping effect of the single-phase pressure drop which is in-phase with the inlet flow perturbation and the destabilizing mechanism of the feedback effect between the kinematic propagation time and the constant pressure drop boundary condition. The two competing effects are separately modelled. The damping effect is modelled by a time-dependent one-dimensional momentum equation, Eq. (1), for the regions including the tube inlet orifice, economizer (EC) and the in-phase part of the evaporator (EV) in the (b1) tube in Fig. 1 [11,24,28]. The destabilizing mechanism of the feedback effect from the constant pressure drop boundary condition of the parallel channel will be reflected by the perturbation of the pressure P_{IP} at the imaginary boundary between the in-phase and out-of-phase parts of the tube.

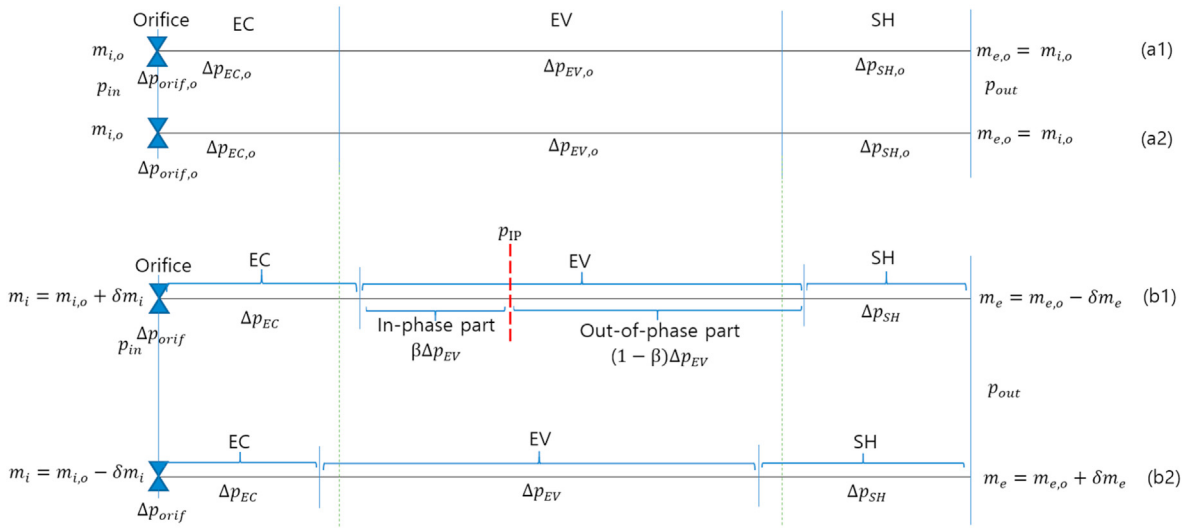

Fig. 1. Schematic representations of coupled parallel channels - steady and perturbed states.

$$\left(\frac{L_{IP}}{A}\right)\frac{dm}{dt} = (P_{in} - P_{IP}) - \Delta P_{orif} - \Delta P_{EC} - \beta \Delta P_{EV} \tag{1}$$

where $\left(\frac{L_{IP}}{A}\right)$ represents an equivalent inertia length for the in-phase part of the tube, m is mass flow rate [kg/sec], P_{in} is the constant inlet header pressure [Pa] of the parallel channel, P_{IP} is the pressure [Pa] at the imaginary boundary dividing the in-phase and out-of-phase parts of the tube as shown in the (b1) tube in Fig. 1, ΔP_{orif} is the pressure drop at the tube inlet orifice [Pa], ΔP_{EC} is the frictional pressure drop in the economizer region [Pa], and $\beta \Delta P_{EV}$ is the frictional pressure drop portion [Pa] in the evaporator region in-phase with the tube inlet single-phase flow perturbation δm_i. Because the frictional pressure drop plays the dominant role in the density wave oscillation and the parallel channel instability in a high thermodynamic quality condition [25], the gravitational head and acceleration pressure drop are not considered in Eq. (1). Because the density wave oscillation and the parallel channel instability become more severe at the low flow operating conditions, the tube inlet orifice size is determined by the lowest flow condition among normal operating conditions. In the lowest flow operating condition, the gravitational head and the acceleration pressure drop are order of magnitude smaller than the frictional pressure drop. Let each variable in Eq. (1) as a sum of a steady state value and a perturbation as follows,

$$\begin{aligned} m &= m_{i,o} + \delta m_i, \\ P_{IP} &= P_{IP,o} + \delta P_{IP}, \\ L_{IP} &= L_{IP,o} + \delta L_{IP}, \\ \Delta P_{orif} &= \Delta P_{orif,0} + \delta \Delta P_{orif}, \\ \Delta P_{orif} &= \Delta P_{orif,0} + \delta \Delta P_{orif}, \\ \Delta P_{EV} &= \Delta P_{EV,0} + \delta \Delta P_{EV} \end{aligned} \tag{2}$$

Putting Eq. (2) into Eq. (1), and taking the first-order perturbation terms out, then Eq. (3) can be obtained

$$\left(\frac{L_{IP,0}}{A}\right)\frac{d(\delta m_i)}{dt} = -\delta P_{IP} - \delta \Delta P_{orif} - \delta \Delta P_{EC} - \beta \delta \Delta P_{EV} \tag{3}$$

The orifice pressure drop term is expressed in terms of steady state and perturbed flow rates as follows.

$$\Delta P_{orif} = K_{orif}\frac{(m_{i,0} + \delta m_i)^2}{2A^2\rho_l} = \Delta P_{orif,0} + \delta \Delta P_{orif} \tag{4}$$

$$\Delta P_{orif,0} = K_{orif}\frac{(m_{i,0})^2}{2A^2\rho_l} \tag{5}$$

$$\delta \Delta P_{orif} = K_{orif}\frac{m_{i,0}\delta m_i}{A^2\rho_l} = 2\Delta P_{orif,0}\frac{\delta m_i}{m_{i,0}} \tag{6}$$

where K_{orif} is the resistance coefficient based on the tube inner diameter, $m_{i,0}$ is the steady state flow rate, δm_i is the tube inlet flow perturbation, A is the inner cross-sectional area of a tube, and ρ_l [kg/m^3] is the fluid density. The second order perturbation terms are neglected.

Similarly, the economizer region pressure drop term can be expressed as

$$\Delta P_{EC} = f_l\frac{L_{EC}}{D}\frac{m_i^2}{2A^2\rho_l} = f_l\frac{(L_{EC,0}+\delta L_{EC})}{D}\frac{(m_{i,0}+\delta m_i)^2}{2A^2\rho_l} = \Delta P_{EC,0} + \delta \Delta P_{EC} \tag{7}$$

$$\Delta P_{EC,0} = f_l\frac{L_{EC,0}}{D}\frac{{m_{i,0}}^2}{2A^2\rho_l} \tag{8}$$

$$\delta \Delta P_{EC} = f_l\frac{L_{EC,0}}{D}\frac{m_{i,0}\delta m_i}{A^2\rho_l} + f_l\frac{\delta L_{EC}}{D}\frac{{m_{i,0}}^2 + 2m_{i,0}\delta m_i}{2A^2\rho_l} \tag{9}$$

where f_l is the friction factor, $L_{EC,0}$ is the length of the economizer region at a steady state [m], δL_{EC} is the length perturbation of the economizer region due to the tube inlet flow perturbation δm_i and D is the tube inside diameter. The second order perturbation terms are neglected.

The heat balances for the economizer region of the steady and perturbed states can be expressed as follows

$$L_{EC,0}\pi D q'' = \left(h_f - h_{in}\right)m_{i,o} \tag{10}$$

$$(L_{EC,0}+\delta L_{EC})\pi Dq'' = \left(h_f - h_{in}\right)(m_{i,0}+\delta m_i) \tag{11}$$

where h_f is the saturation enthalpy of the liquid [J/kg]. The heat flux on the tube surface q'' [W/m^2] and tube inlet enthalpy h_{in} are assumed to be constants. Combining Eq. (10) and Eq. (11), the length perturbation of the economizer region can be expressed as

$$\delta L_{EC} = L_{EC,0}\frac{\delta m_i}{m_{i,0}} \tag{12}$$

Combining Eq. (8), Eq. (9) and Eq. (12) gives us the following expression for the economizer region pressure drop perturbation

$$\delta\Delta P_{EC} = 3\Delta P_{EC,0}\frac{\delta m_i}{m_{i,0}} \tag{13}$$

Similarly, for the evaporator region,

$$\begin{aligned}\beta\delta\Delta P_{EV} &= \beta f_l\frac{L_{EV}}{D}\varnothing_{lo}^2\frac{m_i^2}{2A^2\rho_l} = \beta f_l\frac{(L_{EV,0}+\delta L_{EV})}{D}\varnothing_{lo}^2\frac{(m_{i,0}+\delta m_i)^2}{2A^2\rho_l}\\ &= \beta\Delta P_{EV,0} + \beta\delta\Delta P_{EV}\end{aligned} \tag{14}$$

$$\beta\Delta P_{EV,0} = \beta f_l\frac{L_{EV,0}}{D}\varnothing_{lo}^2\frac{{m_{i,0}}^2}{2A^2\rho_l} \tag{15}$$

$$\beta\delta\Delta P_{EV} = \beta f_l\frac{L_{EV,0}}{D}\varnothing_{lo}^2\frac{m_{i,0}\delta m_i}{A^2\rho_l} + \beta f_l\frac{\delta L_{EV}}{D}\varnothing_{lo}^2\frac{{m_{i,0}}^2+2m_{i,0}\delta m_i}{2A^2\rho_l}, \tag{16}$$

where $\varnothing_{lo}^2$ is the friction pressure drop multiplier [14], β is the ratio of the pressure drop perturbation in the evaporator region in-phase with δm_i and the total pressure drop perturbation in the evaporator region.

The heat balance for the evaporator region gives us an expression for the length perturbation of the evaporator region as follow

$$L_{EV,0}\pi Dq'' = h_{fg}m_{i,o} \tag{17}$$

$$(L_{EV,0}+\delta L_{EV})\pi Dq'' = h_{fg}(m_{i,0}+\delta m_i) \tag{18}$$

$$\delta L_{EV} = L_{EV,0}\frac{\delta m_i}{m_{i,0}} \tag{19}$$

Combining Eq. (15), Eq. (16) and Eq. (19) gives us the following expression for the evaporator region pressure drop perturbation

$$\beta\delta\Delta P_{EV} = 3\beta\Delta P_{EV,0}\frac{\delta m_i}{m_{i,0}} \tag{20}$$

If the pressure P_{IP} at the in-phase and out-of-phase imaginary boundary is determined (see Fig. 1), because the multichannel outlet header pressure P_{out} is constant, the force balance in the out-of-phase portion of the tube can be written as

$$(P_{IP} - P_{out})A = \{(1-\beta)\Delta P_{EV} + \Delta P_{SH}\}A \tag{21}$$

where ΔP_{SH} is the frictional pressure drop in the superheater region [Pa]. Putting Eq. (2) and Eq. (22) into Eq. (21), we get Eq. (23).

$$\Delta P_{SH} = \Delta P_{SH,0} + \delta\Delta P_{SH}, \tag{22}$$

$$\delta P_{IP} = (1-\beta)\delta\Delta P_{EV} + \delta\Delta P_{SH} \tag{23}$$

The out-of-phase portion of the evaporator region pressure drop can be expressed as a function of the tube outlet flow rate and the perturbation of the outlet flow rate as follow.

$$\begin{aligned}(1-\beta)\delta\Delta P_{EV} &= (1-\beta)f_l\frac{L_{EV}}{D}\varphi_{lo}^2\frac{{m_e}^2}{2A^2\rho_l}\\ &= (1-\beta)f_l\frac{(L_{EV,0}+\delta L_{EV})}{D}\varphi_{lo}^2\frac{(m_{e,0}-\delta m_e)^2}{2A^2\rho_l}\\ &= (1-\beta)\Delta P_{EV,0} + (1-\beta)\delta\Delta P_{EV}\end{aligned} \tag{24}$$

$$(1-\beta)\Delta P_{EV,0} = (1-\beta)f_l\frac{L_{EV,0}}{D}\varnothing_{lo}^2\frac{{m_{e,0}}^2}{2A^2\rho_l} \tag{25}$$

$$\begin{aligned}(1-\beta)\delta\Delta P_{EV} = &-(1-\beta)f_l\frac{L_{EV,0}}{D}\varnothing_{lo}^2\frac{m_{e,0}\delta m_e}{A^2\rho_l}\\ &+ (1-\beta)f_l\frac{\delta L_{EV}}{D}\varnothing_{lo}^2\frac{{m_{e,0}}^2-2m_{e,0}\delta m_e}{2A^2\rho_l}\end{aligned} \tag{26}$$

where $m_{e,0}$ is the steady state tube outlet flow rate which is equal to $m_{i,0}$. Note that the tube outlet flow perturbation δm_e has a negative sign which means 180° out-of-phase with the positive tube inlet flow perturbation δm_i [24]. Similar with Eq. (17), Eq. (18) and Eq. (19), the heat balance for the out-of-phase evaporator region gives us an expression for the length perturbation of the evaporator region in terms of $m_{e,0}$ and δm_e as follow,

$$\delta L_{EV} = -L_{EV,0}\frac{\delta m_e}{m_{e,0}} \tag{27}$$

Combining Eq. (25), Eq. (26) and Eq. (27) gives us the following expression for the evaporator region pressure drop perturbation,

$$(1-\beta)\delta\Delta P_{EV} = -3(1-\beta)\Delta P_{EV,0}\frac{\delta m_e}{m_{e,0}} \tag{28}$$

The superheater region pressure drop term can be expressed as

$$\Delta P_{SH} = f_v\frac{L_{SH}}{D}\frac{{m_e}^2}{2A^2\rho_v} = f_v\frac{(L_{SH,0}+\delta L_{SH})}{D}\frac{(m_{e,0}-\delta m_e)^2}{2A^2\rho_v} = \Delta P_{SH,0}+\delta\Delta P_{SH} \tag{29}$$

$$\Delta P_{SH,0} = f_v\frac{L_{SH,0}}{D}\frac{{m_{e,0}}^2}{2A^2\rho_v} \tag{30}$$

$$\delta\Delta P_{SH} = -f_v\frac{L_{SH,0}}{D}\frac{m_{e,0}\delta m_e}{A^2\rho_v} + f_v\frac{\delta L_{SH}}{D}\frac{{m_{e,0}}^2-2m_{e,0}\delta m_e}{2A^2\rho_v} \tag{31}$$

The heat balance for the superheater region of the steady and perturbed states can be expressed as follows

$$L_{SH,0}\pi Dq'' = \Delta h_{SH,0}m_{e,o} \tag{32}$$

$$(L_{SH,0}+\delta L_{SH})\pi Dq'' = (\Delta h_{SH,0}+\delta\Delta h_{SH})(m_{e,0}-\delta m_e) \tag{33}$$

where $L_{SH,0}$ is the length of the superheater region at a steady state, δL_{SH} is the length perturbation of the superheater region due to the flow perturbation δm_e, $\Delta h_{SH,0}$ is the enthalpy rise in the superheater region at a steady state, and $\delta\Delta h_{SH}$ is the perturbation of the enthalpy rise in the superheater region. Combining Eq. (32) and Eq.

(33), we can get the superheater length perturbation equation as

$$\delta L_{SH} = L_{SH,0}\left\{ -\frac{\delta m_e}{m_{e,0}} + \frac{\delta \Delta h_{SH}}{\Delta h_{SH,0}} \right\} \tag{34}$$

In Eq. (34), the superheater enthalpy perturbation term $\delta \Delta h_{SH}$ can be neglected for the tube inlet orifice sizing purpose. It is because the tube inlet orifice size is determined at low flow operating conditions. When an OTSG is operating at low flow conditions, the superheater region length amounts to almost 80–90% of the total tube length and the superheated steam temperature does not practically change which is almost the same with the primary side hot temperature. Thus, the steam exit enthalpies for the $m_{e,0}$ and $m_{e,0} - \delta m_e$ flow conditions are almost the same. Eq. (34) can be written as

$$\delta L_{SH} = -L_{SH,0}\frac{\delta m_e}{m_{e,0}} \tag{35}$$

Combining Eqs. (3), (6), (13), (20), (23), (28) and (35), we can reform Eq. (3) in terms of steady state frictional pressure drop terms and flow perturbations as follow.

$$\left(\frac{L_{IP,0}}{A}\right)\frac{d(\delta m_i)}{dt} = 3\,\frac{\delta m_e}{m_{e,0}}\left\{\Delta P_{SH,0} + (1-\beta)\Delta P_{EV,0}\right\} - \left\{2\Delta P_{orif,0} + 3\Delta P_{EC,0} + 3\beta\Delta P_{EV,0}\right\}\frac{\delta m_i}{m_{i,0}} \tag{36}$$

Because $m_{e,0}$ is equal to $m_{i,0}$ for a steady state, Eq. (36) can be written as

$$\left(\frac{L_{IP,0}}{A}\right)\frac{d\{\ln(\delta m_i)\}}{dt} = \frac{3}{m_{i,0}}\left[\left\{\Delta P_{SH,0} + (1-\beta)\Delta P_{EV,0}\right\}\frac{\delta m_e}{\delta m_i} - \left\{\frac{2}{3}\Delta P_{orif,0} + \Delta P_{EC,0} + \beta\Delta P_{EV,0}\right\}\right] \tag{37}$$

For a stable operation of parallel-channel steam generating systems and decaying out of the tube inlet flow perturbation, the righthand side of Eq. (37) should be negative. From this criterion, the tube inlet orifice can be sized with the following equation.

$$\Delta P_{orif,0} \geq \frac{3}{2}\left\{\Delta P_{SH,0} + (1-\beta)\Delta P_{EV,0}\right\}\frac{\delta m_e}{\delta m_i} - \frac{3}{2}\left(\Delta P_{EC,0} + \beta\Delta P_{EV,0}\right) \tag{38}$$

3. Discussions

Petrov [19] claimed that parallel steam generating channels can be operated stably when the following criterion is satisfied

$$K_{Petrov} \equiv \frac{\Delta P_{orif} + \Delta P_{EC}}{\Delta P_{SH} + \Delta P_{EV}} \geq 1 \tag{39}$$

where K_{Petrov} is defined as an orifice coefficient [19–21], ΔP_{orif} is a pressure drop at the tube inlet orifice, ΔP_{EC} is the pressure drop at the economizer region, ΔP_{EV} is the pressure drop at the evaporator region, and ΔP_{SH} is the pressure drop at the superheater region of the tube. In many subsequent applications of this criterion, the orifice coefficient K_{Petrov} turns out to have a wide range of variation for various facilities [20–23]. In the Kang's [21] and Han's [22] papers, the adopted orifice coefficient is 1.92 based on test data and experience rather than 1.0 in Eq. (39) [20].

Fig. 2 shows experimental data [20,21] for the KLT-40 Russian reactor OTSGs. The experiments are performed for the primary coolant mass fluxes 500 and 1700 kg/m^{2}sec, for the range of the secondary coolant mass fluxes, 88–264kg/m^{2}sec, and for the 15, 20, 25, and 30 kgf/cm^2 steam pressure conditions. In the Figure, the orifice coefficients are calculated values using Eq. (39) for each experimental condition. For the 15 and 20 kgf/cm^2 steam pressure conditions, the measured flowrate fluctuation magnitudes are scattered up to the 100% rated feedwater flowrate. The variation of the primary coolant mass flux turns out not to affect on the fluctuation magnitudes much. The scattered fluctuation magnitudes for the 15 and 20 kgf/cm^2 steam pressure conditions are mainly due to the different magnitudes of the feedwater mass flux 88–264 kg/m^{2}sec, the smaller feedwater flow rate the higher fluctuation magnitude [20]. The test data trend in Fig. 2 shows that the flow rate fluctuation magnitudes decrease as the steam pressure increases and the orifice coefficient becomes large. The K_{Petrov} value 1.92 is chosen for the conservative orifice sizing purpose from the data trend in Fig. 2 [20–22], even though Petrov recommended 1.0 in Eq. (39).

The tube inlet orifice sizing criterion, Eq. (38), can be reformed to compare with the Petrov's criterion, Eq. (39), as follow.

$$K_{Yoon} = \frac{\Delta P_{orif,0} + \frac{3}{2}\left(\Delta P_{EC,0} + \beta\Delta P_{EV,0}\right)}{\left\{\Delta P_{SH,0} + (1-\beta)\Delta P_{EV,0}\right\}\frac{\delta m_e}{\delta m_i}} \geq \frac{3}{2} \tag{40}$$

Comparing Eq. (39) and Eq. (40), the two equations become most similar when $\beta = 0$ and $\frac{\delta m_e}{\delta m_i} = 1$. These values are reasonable assumptions. In case of $\beta = 0$, because the channel void fraction increases very steeply with the initial thermodynamic quality increase [14,33], it is natural assuming that the whole pressure drop perturbation of the evaporator region is in-phase with that of the superheater region. Also, the $\frac{\delta m_e}{\delta m_i} = 1$ means that the magnitude of the steam mass flowrate perturbation at the tube outlet is limited by the magnitude of the tube inlet flowrate perturbation at the stability threshold. With these assumptions, Eq. (40) becomes

$$K_{Yoon} = \frac{\Delta P_{orif,0} + \frac{3}{2}\Delta P_{EC,0}}{\Delta P_{SH,0} + \Delta P_{EV,0}} \geq \frac{3}{2} \tag{41}$$

Comparing Eq. (39) and Eq. (41), it can be realized that the Petrov's orifice coefficient should be greater than 1.5 rather than 1.0. This difference is originated from modelling of the heat transfer regime boundary perturbations. Petrov neglected the effects of the heat transfer regime boundary perturbations, and he had only considered the pressure drop perturbations due to the flow rate perturbations in each heat transfer regime region with a constant pressure drop boundary condition between the parallel channel headers. The factor 3/2 of the $\Delta P_{EC,0}$ term in Eq. (41) came from the modelling of the economizer region boundary perturbation.

The ONCESG code [29] is utilized to simulate the SMART OTSG [30–32]. Fig. 3 shows frictional pressure drops in each economizer, evaporator and superheater region for steam pressure 5.76–6.65 MPa and 3.5 MPa cases. The higher steam pressure range 5.76–6.65 MPa is the operating steam pressure of the SMART reactor, and the steam pressure 3.5 MPa is selected to investigate a sensitivity of the new criterion K_{Yoon} on the steam pressure variation. The range of the feedwater flow rate is 58.8–559.7 kg/m^{2}sec which corresponds to the 12%–100% rated power range of the SMART reactor. In an OTSG, the feedwater flow rate and the corresponding heat transfer power level have an almost linear relationship because the latent heat of the water is order of magnitude larger than the heat transferred in the economizer and superheater

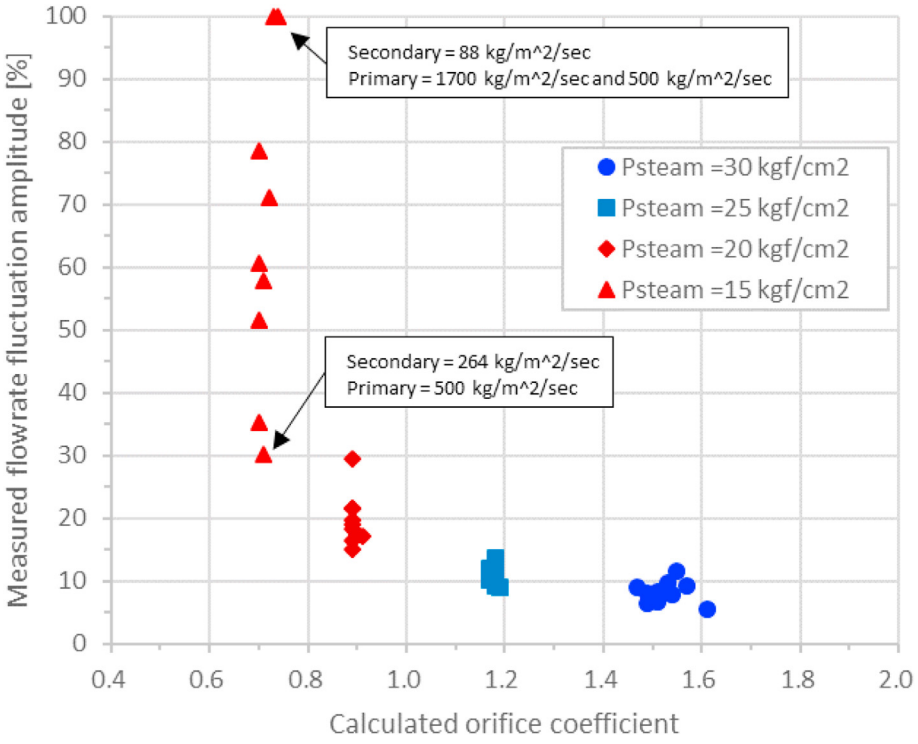

Fig. 2. Model test results for the KLT-40 reactor OTSG.

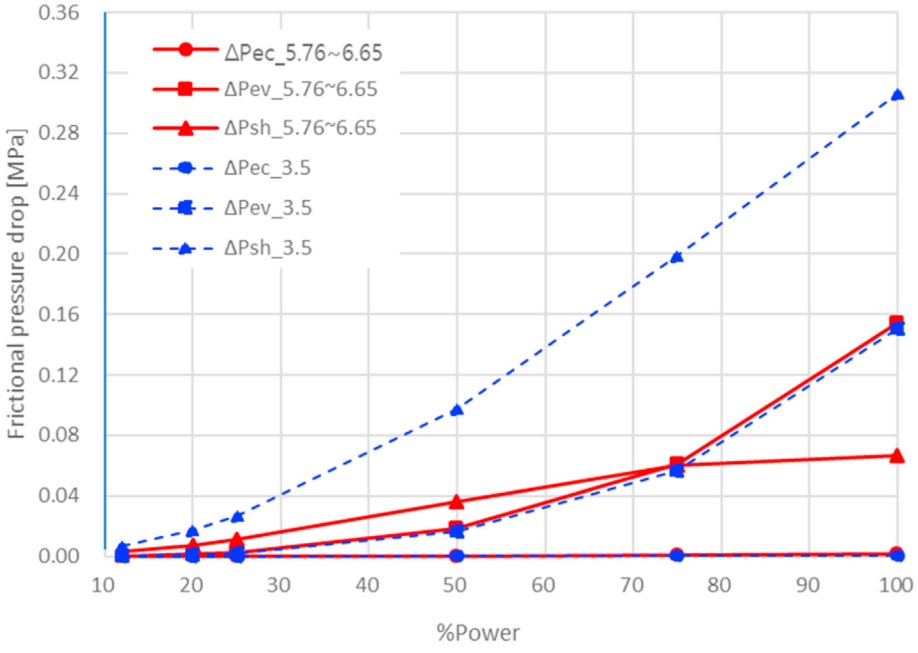

Fig. 3. Regional friction pressure drop for 5.76–6.65 MPa and 3.5 MPa steam pressure cases.

regions. The economizer region pressure drops are order of magnitude smaller than evaporator and superheater region pressure drops for both steam pressure ranges. The superheater region pressure drop ratio of two different steam pressures, $\frac{\Delta P_{SH,3.5MPa}}{\Delta P_{SH,5.76\sim6.65MPa}}$, ranges from 2.3 to 4.6. It means that the low steam pressure cases are more susceptible to the parallel channel instability, because the superheater region pressure drop is 180° out-of-phase with the tube inlet flow perturbation.

Fig. 4 shows orifice coefficients for steam pressures 5.76–6.65 MPa and 3.5 MPa calculated by using Eq. (40) and regional friction pressure drops calculated by the ONCESG code as shown in Fig. 3. The orifice pressure drop ΔP_{orif} in Eq. (40) is calculated by using Eq. (38) rather than a pressure drop at an installed specific orifice for a steam generator. This means a right size of an orifice to suppress the parallel channel instability is assumed for each corresponding feedwater flowrate. In Fig. 4, the

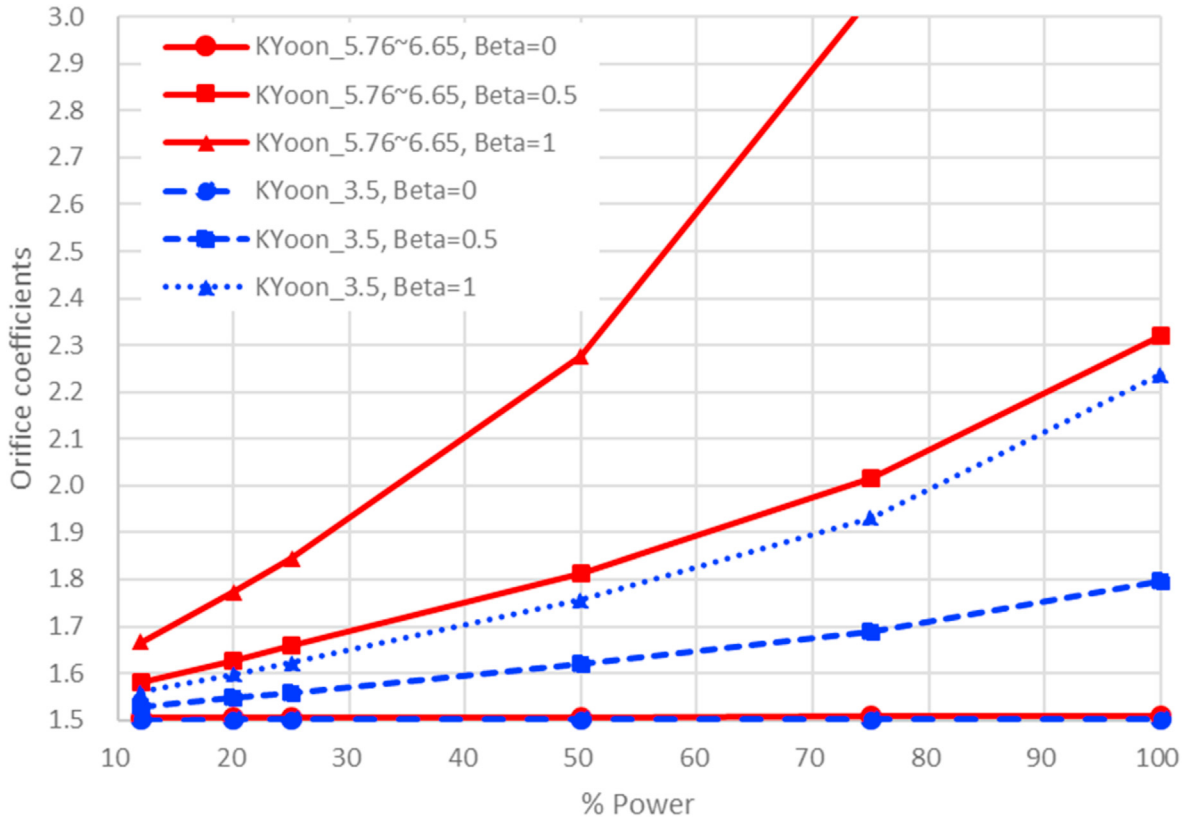

Fig. 4. orifice coefficients for varying steam pressures and β values.

outlet and inlet flow rate perturbation ratio $\frac{\delta m_e}{\delta m_i}$ is assumed to be 1, and it is a reasonable assumption for the stability threshold. The orifice coefficient K_{Yoon} is plotted for $\beta = 0$, 0.5, and 1. The orifice coefficient approach to the factor 3/2 as the feedwater flow rate decreases in Fig. 4. As can be seen in Fig. 3, the economizer and evaporator region pressure drops become negligible as the feedwater flow rate decreases. Eq. (40) shows that K_{Yoon} converges to the ratio of $\frac{\Delta P_{orif}}{\Delta P_{SH}\frac{\delta m_e}{\delta m_i}}$ as the feedwater flow rate decreases, and Eq. (38) says this ratio converges to $\frac{3}{2}$.

Fig. 5 shows the required orifice pressure drop calculated by using Eq. (38) for the two steam pressure ranges 5.76–6.65 MPa and 3.5 MPa and for the value $\beta = 0,\ 0.5$ and 1 as a function of the percent rated power. In Eq. (38), $\frac{\delta m_e}{\delta m_i}$ is assumed to be 1.0. Thin dotted lines and thick dotted lines correspond to the lines representing the orifice pressure drops with $\beta = 0.5$ and 1, respectively. Solid lines are for $\beta = 0$. Fig. 5 shows that the effects of the β value variation on the required orifice pressure drops are minor for the low flow conditions. It is because the evaporator region pressure drop ΔP_{EV} is order of magnitude smaller than the superheater region pressure drop ΔP_{SH} for a low flow condition. As expected, the calculated threshold orifice pressure drop is very small for low feedwater flow cases. When sizing the tube inlet orifice, one important design consideration is the orifice pressure drop at the rated feedwater flow rate, which determines the feedwater pump specifications. Fig. 5 also shows the orifice pressure drop with the 100% feedwater flow rate for each orifice sized for a specific feedwater flow rate. For example, the required orifice pressure drop for the 12% rated power at the 5.76–6.65 MPa steam pressure is calculated to be 5.0 kPa by Eq. (38) with $\beta = 0$ and $\frac{\delta m_e}{\delta m_i} = 1$. If the corresponding orifice is installed at the tube inlet and the steam generator is operating with the 100% rated feedwater flow rate, the pressure drop at the orifice will be $5.0*(9.52)^2 = 454$ kPa, where the number 9.52 is the ratio of the feed water flow rate at the 100% rated power to the feedwater flow rate at the 12% rated power in the SMART OTSG. The corresponding orifice pressure drop becomes 432 kPa and 410 kPa for $\beta = 0.5$ and $\beta = 1$, respectively, as shown in Fig. 5. By definition, $\beta = 0$ means that the whole pressure drop perturbation in the evaporator region is 180° out-of-phase with the inlet feedwater flow perturbation δm_i, and the $\beta = 0$ case predicts a larger tube inlet orifice which is conservative in the flow stability points of views compared with the $\beta = 0.5$ and $\beta = 1$ cases. Also, a reasonable value for the β value will be close to 0, because the void fraction increases steeply at very low thermodynamic quality in boiling channels [14,33]. If the target operating steam pressure is 3.5 MPa, the orifice should be sized to have a pressure drop of 977.8 kPa at the 100% rated feedwater flow rate as shown in Fig. 5. This large irreversible orifice pressure drop can be a burden for the feedwater pumping power for the plant life time. If the 3.5 MPa steam pressure is necessary for a startup process only, for example, the orifice can be sized for the 5.76–6.65 MPa operating steam pressure range, and the operating time at the 3.5 MPa steam pressure can be shortened during the startup process.

In Kang's study [21], he sized the tube inlet orifice using the K_{Petrov} formula with the 92% margin, i.e., $K_{Petrov} = 1.92$. Because the minimum operating power of the SMART is the 12% of the rated power, utilizing the ONCESG calculation results shown in Fig. 3 and Eq. (39), the corresponding orifice pressure drop is calculated to be 6.4 kPa at the 12% rated power, and it corresponds to 580 kPa ($=6.4$ kPa$*(9.52)^2$) at the rated power, where the number 9.52 is the ratio of the feed water flow rate at the 100% rated power to that at

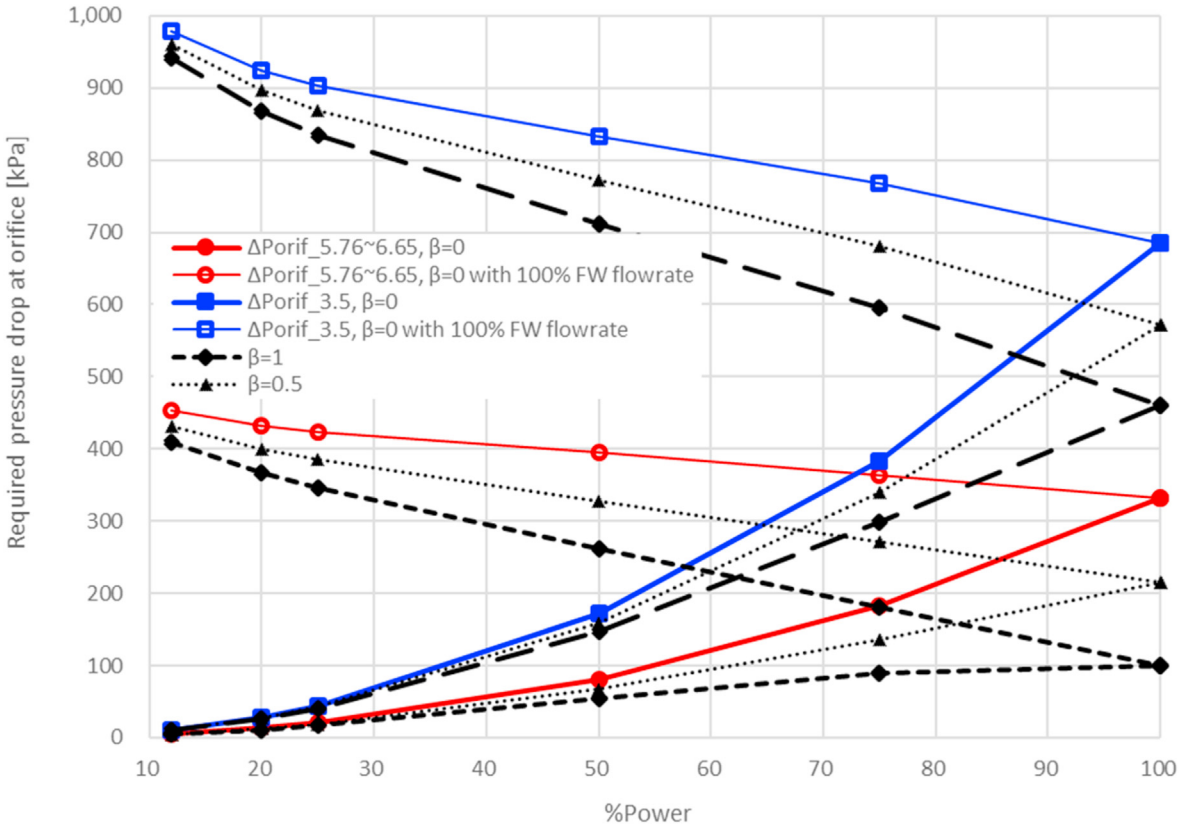

Fig. 5. Required pressure drop at the tube inlet orifice with β = 0, 0.5, 1 and $\frac{\delta m_e}{\delta m_i} = 1$.

the 12% rated power in the SMART OTSG.

The K_{Yoon} criterion Eq. (38) predicted the required orifice pressure drop of 5 kPa at the 12% rated power for the 5.76–6.65 MPa operating steam pressure range, which is equivalent to 454 kPa for the rated power operation as can be seen in Figs. 5 and 6, and this value is less than the 580 kPa calculated by K_{Petrov}. Fig. 6 is a detailed view for the low power range in Fig. 5. The ambiguous 92% engineering margin in the K_{Petrov} criterion based on experience and experimental data is justified to be conservative enough by this calculation.

Nariai et al. [24] presented the stability threshold for an OTSG based on their extensive experimental data. The Nariai's stability threshold can be reformed in notations defined in this paper as follow

$$\frac{\Delta P_{orif}}{\Delta P_{SH} + P_{EV}} = \left\{(1-\beta)\left(\frac{\Delta P_{EV}}{\Delta P_{SH} + P_{EV}}\right) + \frac{\Delta P_{SH}}{\Delta P_{SH} + P_{EV}}\right\} \frac{\delta m_e}{\delta m_i} \tag{42}$$

Eq. (42) can be rearranged as

$$\Delta P_{orif} = \{\Delta P_{SH} + (1-\beta)\Delta P_{EV}\} \frac{\delta m_e}{\delta m_i} \tag{43}$$

Comparing Eqs. (43) and (38), the factor 3/2 and the second term of the righthand side of Eq. (38) are missing in the righthand side of Eq. (43). The factor 3/2 is missing in Eq. (43), because Nariai et al. did not model the phase boundary perturbations due to the tube inlet flow perturbation. The second term of the righthand side of Eq. (38) is missing in the righthand side of Eq. (43), because Nariai et al. neglected the pressure drop perturbation in the economizer region.

Nariai et al. [24] presented an empirical formula for the term $\frac{\delta m_e}{\delta m_i}$ and graphical data to read the K_{orif} value to calculate the pressure drop at the orifice for the stability threshold as functions of L_{EV}/L_T, where L_{EV} is the evaporator region length and L_T is the total tube length. However, both the formula for $\frac{\delta m_e}{\delta m_i}$ and the graphical data to read the K_{orif} are given for the range $L_{EV}/L_T > 0.2$. As mentioned previously, the tube inlet orifice size should be determined for a normal operating condition having the lowest flow rate and the lowest steam pressure, in which the parallel channel instability should be prevented. Fig. 7 shows the tube length occupied by the economizer and evaporator regions as a function of the percent

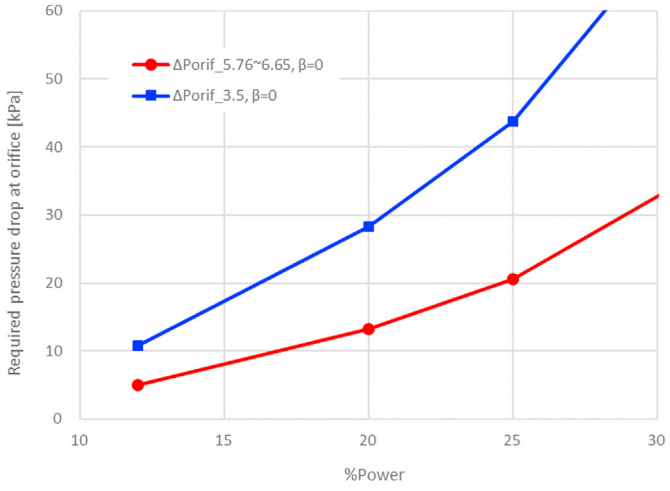

Fig. 6. Required pressure drop at the tube inlet orifice (low flow range) with β = 0 and $\frac{\delta m_e}{\delta m_i} = 1.0$.

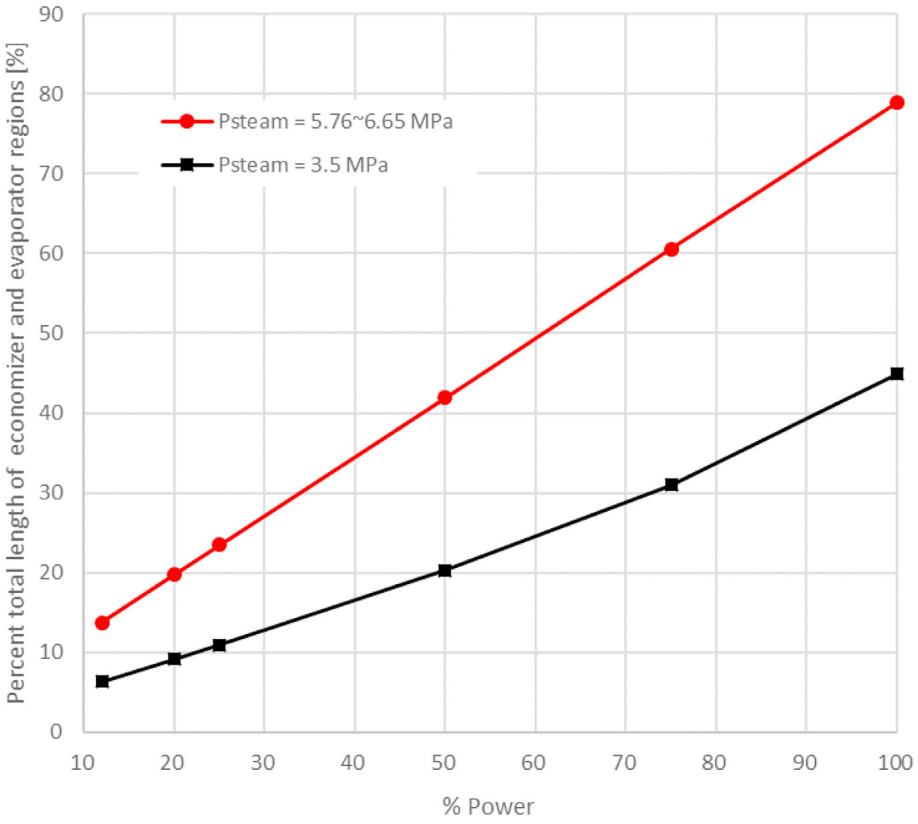

Fig. 7. $(L_{EC}+L_{EV})/L_T$ as a function of a percent power.

power for two steam pressure ranges 5.76–6.65 MPa and 3.5 MPa. In the Nariai's model, the economizer region L_{EC} is not modelled, thus they used L_{EV}/L_T rather than $(L_{EC}+L_{EV})/L_T$. As can be seen in Fig. 7, the value $(L_{EC}+L_{EV})/L_T$ is below 20% for the 20% and below power operating conditions. It means that the Nariai's model cannot be utilized for sizing the tube inlet orifice for the 20% and below power operating conditions. The Nariai's formulation is for representing their experimental data, but not practical for sizing the tube inlet orifice for an OTSG.

4. Conclusion

The newly proposed model confirmed that the tube inlet orifice pressure drop and the superheater region pressure drop are major players in the parallel channel instability of an OTSG. It explains that many stability thresholds derived for the BWR cores cannot be utilized for the OTSG orifice design, because these models do not have the superheater region model.

This paper identifies the perturbation model of the heat transfer regime boundaries as a missing part of the existing models based on the perturbation model, Petrov's criterion and Nariai's model. Because of this missing part, Petrov's criterion underestimates by about 50% the necessary pressure drop at the tube inlet orifice of an OTSG to suppress the parallel channel instability. This inaccuracy of the Petrov's model has made engineers consider additional conservative margin in the orifice pressure drop, and using ambiguous large margin became a common practice.

The proposed model predicts the required tube inlet orifice size to suppress the parallel channel instability without unnecessary margin.

Declaration of competing interest

The author declares no conflict of interest.

Acknowledgement

This work was supported by the National Research Foundation of Korea (NRF) funded by the Korea government (Ministry of Science and ICT) (No. NRF-2020M2D7A1079178).

Appendix A. Supplementary data

Supplementary data to this article can be found online at https://doi.org/10.1016/j.net.2021.06.003.

References

[1] M. Xiao, X.J. Chen, M.Y. Zhang, T.N. Veziroglu, S. Kakac, A multivariable linear investigation of two-phase flow instabilities in parallel boiling channels under high pressure, Int. J. Multiphas. Flow 19 (1) (1993) 65–77.
[2] G.V. Durga Prasad, M. Pandey, M.S. Kalra, Review of research on flow instabilities in natural circulation boiling systems, Prog. Nucl. Energy 49 (2007) 429–451.
[3] J.A. Boure, Review of two-phase flow instability, Nucl. Eng. Des. 25 (1973) 165–192.
[4] K. Fukuda, S. Hasegawa, Analysis on two-phase flow instability in parallel multichannels, J. Nucl. Sci. Technol. 16 (3) (1979) 190–199.
[5] L.C. Ruspini, C.P. Marcel, A. Clausse, Two-phase flow instabilities: a review, Int. J. Heat Mass Tran. 71 (2014) 521–548.
[6] M. Ishii, Thermally Induced Flow Instabilities in Two-phase Mixtures in Thermal Equilibrium, Ph.D. Thesis, GIT, 1971.
[7] L.A. Belblidia, Density-wave oscillations, Ann. Nucl. Energy 6 (1979) 425–444.
[8] Dag Strømsvag, Fundamental Mechanisms of Density Wave Oscillations and the Effect of Subcooling, NTNU, 2004.
[9] P. Saha, An experimental investigation of the thermally induced flow oscillations in two-phase systems, J. Heat Tran. (1976) 616–622.

[10] K. Takitani, T. Takemura, Density wave instability in once-through boiling flow system, (I) Experiment, J. Nucl. Sci. Technol. 15 (5) (1978) 355–364.
[11] K. Takitani, Density wave instability in once-through boiling flow system, (II) Lumped parameter model with moving boundaries, J. Nucl. Sci. Technol. 15 (6) (1978) 389–399.
[12] K. Takitani, K. Sakano, Density wave instability in once-through boiling flow system, (III) Distributed parameter model, J. Nucl. Sci. Technol. 16 (1) (1979) 16–29.
[13] G. Guido, et al., Density-wave oscillations in parallel channels – an analytical approach, Nucl. Eng. Des. 125 (1991) 121–136.
[14] R.T. Lahey Jr., The Thermal-Hydraulics of a Boiling Water Nuclear Reactor, second ed., ANS, 1993.
[15] M. Colombo, A. Cammi, D. Papini, M.E. Ricotti, RELAP5/MOD3.3 study on density wave instabilities in single channel and two parallel channels, Prog. Nucl. Energy 56 (2012) 15–23.
[16] G. Xia, M. Peng, Y. Guo, Research of two-phase flow instability in parallel narrow multi-channel system, Ann. Nucl. Energy 48 (2012) 1–16.
[17] R. Xu, P. Song, D. Zhang, W. Tian, S. Qiu, G. Su, Numerical analysis on flow instability of parallel channels in steam generator for sodium-cooled fast reactor, Int. J. Energy Res. (2020) 1–14.
[18] Q. Liang, X. Li, Y. Su, X. Wu, Frequency Domain Analysis of Two-phase Flow Instabilities in a Helical Tube once through Steam Generator for HTGR vol. 168, Applied Thermal Eng., 2020.
[19] P.A. Petrov, Hydrodynamics of Once-Through Boiler, 1960. Gosenergoizdat (in Russian).
[20] V.A. Babin, Final Report on Problems of Ensuring the Hydrodynamic Stability of the Once-Through Steam Generators in Normal Operating Modes, OKBM, 2004.
[21] H.O. Kang, J.K. Seo, Y.W. Kim, J. Yoon, K.K. Kim, Structural integrity confirmation of a once-through steam generator from the viewpoint of flow instability, J. Nucl. Sci. Technol. 44 (1) (2007) 64–72.
[22] H.S. Han, Rayan Alshehri, H.O. Kang, J. Yoon, Y.I. Kim, S.J. Kim, Tube inlet orifice design of a once-through steam generator for flow stabilization, J. Mech. Sci. Technol. 33 (8) (2019) 3841–3849.
[23] Huaiming Ju, K. Zuo, Z. Liu, Y. Xu, Two phase flow stability in HTR-10 steam generator, Tsinghua Sci. Technol. 6 (1) (2001) 75–79. ISSN 1007–0214, 16/20.
[24] H. Nariai, M. Kobayashi, T. Matsuoka, Y. Ito, I. Aya, Boiler dynamics and control in nuclear power stations 2, Ch. 14 Flow instabilities in a once-through steam genertor, in: Proceedings of the Second International Conference Held in Bournemouth, The British Nuclear Energy Society, London, 1980, pp. 23–25. October, 1979.
[25] K. Fukuda, T. Kobori, Classification of two-phase flow instability by density wave oscillation model, J. Nucl. Sci. Technol. 16 (2) (1979) 95–108.
[26] P.K. Vijayan, A.K. Nayak, ANNEX 7 Introduction to Instabilities in Natural Circulation systems, IAEA-TECDOC-1474 Natural Circulation in Water Cooled Nuclear Power Plants, IAEA, 2005.
[27] R.T. Lahey Jr., M.Z. Podowski, On the analysis of various instabilities in two-phase flows, Multiphas. Sci. Technol. 4 (1989) 183–370.
[28] N.E. Todreas, M.S. Kazimi, Nuclear Systems I: Thermal Hydraulic Fundamentals, second ed., Hemisphere Publishing Co., 2011.
[29] Juhyeon Yoon, J.P. Kim, H.Y. Kim, D.J. Lee, M.H. Chang, Development of a computer code, ONCESG, for the thermal-hydraulic design of a once-through steam generator, J. Nucl. Sci. Technol. 37 (5) (2000) 445–454.
[30] H.K. Kim, S.H. Kim, Y.J. Chung, H.S. Kim, Thermal-hydraulic analysis of SMART steam generator tube rupture using TASS/SMR-S code, Ann. Nucl. Energy 55 (2013) 331–340.
[31] Y.W. Kim, J.I. Kim, D.O. Kim, J.S. Park, H.S. Lee, Basic design report for SMART steam generator, KAERI/TR-2127, INIS Issue 47 (2002) http://inis.iaea.org/, INIS Vol. 35.
[32] M.H. Chang, J.W. Yeo, Q.S. Zee, D.J. Lee, K.B. Park, I.S. Koo, H.C. Kim, J.I. Kim, Basic design report of SMART, INIS Issue 36 (2002). INIS Vol. 34, http://inis.iaea.org/.
[33] P.K. Vijayan, A.P. Patil, D.S. Pilkhwal, D. Saha, V. Venkat Raj, An assessment of pressure drop and void fraction correlations with data from two-phase natural circulation loops, Heat Mass Tran. 36 (2000) 541–548.